

Large calculated electron-phonon interactions in $\text{La}_{2-x}\text{M}_x\text{CuO}_4$

H. Krakauer

Department of Physics, College of William and Mary, P.O. Box 8795, Williamsburg, Virginia 23187-8795

W. E. Pickett

Complex Systems Theory Branch, Code 6690, Naval Research Laboratory, Washington, D.C. 20375-5320

R. E. Cohen

Geophysical Laboratory, Carnegie Institution of Washington, 5251 Broad Branch Road, N.W. Washington, D.C. 20015-1305

(Received 29 June 1992)

Results of self-consistent linearized-augmented-plane-wave calculations within the local-density-functional approximation (LDA) are presented of the electron-phonon-induced linewidths and interaction strength of selected phonons in $\text{La}_{2-x}\text{M}_x\text{CuO}_4$ at $x=0.15$. Through the use of a supercell geometry, rigid-ion-type approximations are avoided and the full electron-phonon matrix elements are determined from finite differences of the LDA potentials corresponding to frozen-in phonon at Γ , X , and Z . At the X point, all fully symmetric A_g modes (i.e., having the symmetry of the oxygen planar-breathing mode) as well as three modes having B_{3g} symmetry are examined. Small linewidths were found for the three B_{3g} modes, and moderate linewidths for the A_g modes, the largest corresponding to ratios $\gamma_{q,v}/\omega_{q,v}=0.02$ for the oxygen breathing and axial modes. The axial O_z mode at the Z point has a very large width, $\gamma_{q,v}/\omega_{q,v}=0.11$. Unusual long-range Madelung-like interactions are found to yield large matrix elements, especially for modes near the zone center and are responsible for couplings of the cations (La) to the charge carriers. The linewidth of a mode also directly determines $\lambda_{q,v}$, the contribution of mode (q,v) to the electron-phonon coupling constant, λ , and an approximate average over the Brillouin zone yields $\lambda \approx 1.3$, about the magnitude necessary to explain T_c in $\text{La}_{2-x}\text{M}_x\text{CuO}_4$. In spite of some very strong coupling to low-frequency modes, the mean frequency ω_{\log} that is important in determining T_c is large: $\omega_{\log}=321 \text{ cm}^{-1}=462 \text{ K}$. The calculated large electron-phonon coupling arises from a combination of weak screening and unusual nonlocal Madelung-like interactions, in concert with strong Cu-O hybridization that results in good metallic behavior within the planes. These features are common to all of the layered cuprates, indicating that the entire class should show strong electron-phonon coupling.

I. INTRODUCTION

Since the discovery of the high-temperature cuprate superconductors by Bednorz and Müller,¹ the number of theories seeking to explain the exceptionally high values of the transition temperature, T_c , has grown dramatically. Many theories, based on the Hubbard model, have suggested that an electronic rather than a conventional electron-phonon mechanism is responsible for the superconducting pairing. This development was due in part to early experiments that failed to find evidence of a Fermi surface in these materials and in part to the existence of nearby insulating phases. Thus it seemed quite reasonable to regard the superconducting phases as doped Mott insulators.

Recently, however, the unmistakable observations of a Fermi surface by several experimental methods and the observation, by direct and inverse photoemission, of a continuous spectra density above and below the Fermi energy, E_F , rule out this earlier scenario. These results, in very good agreement with band theory, strongly support Fermi-liquid behavior in the normal state and severely constrain possible theories of the high-temperature superconductors.² While these experiments do not, of course, rule out an electronic mechanism, they

do require that any theory agree with the observed normal state characteristics of the metallic (and superconducting) phase. Since band theory, i.e., the local density functional approximation (LDA),³ satisfies this constraint, it is reasonable to regard the LDA results as a starting point for describing the low-energy electronic excitations as is done in more conventional materials. This in turn has led to serious reconsideration of the electron-phonon mechanism as at least partly responsible for superconductivity.⁴ Ironically, strong electron-phonon coupling is what originally motivated investigating the transition metal oxides.⁵ There has long been evidence of strong electronic coupling to vibrational modes from a variety of experimental probes,⁶⁻⁸ and recently Landau damping of phonon modes in $\text{YBa}_2\text{Cu}_3\text{O}_7$ has been observed⁹ that is generally consistent with the band picture. In this paper we present *ab initio* linearized augmented plane wave (LAPW)¹⁰ calculations that provide evidence of very strong electron-phonon interactions that may be large enough to account for T_c in $\text{La}_{2-x}\text{M}_x\text{CuO}_4$.

Unfortunately, the evaluation of the electron-phonon interaction strength for the high- T_c superconductors (HTSC) is a difficult problem. The commonly used rigid-ion (RI) and rigid muffin-tin (RMT) approximations are not adequate for these materials. The RI and RMT ap-

proximations neglect changes in the potential everywhere except on the atom that is displaced. For isotropic metals that have a large density of state at the Fermi energy, $\rho(E_F)$, these approximations work well in many cases,¹¹ since the efficient electronic screening limits the change in the potential to the immediate vicinity of the atom that is displaced. By contrast, in the HTSC's the combination of an anisotropic structure and small $\rho(E_F)$ results in large nonlocal or off-site contributions to the electron-phonon coupling. Weak screening permits large Madelung-like shifts in potential (and hence coupling) from all ions. In $\text{YBa}_2\text{Cu}_3\text{O}_7$, for example, the RMT approximation gives negligible contributions¹² from the Ba atoms, because there are virtually no electronic states at the Fermi energy on these atoms, and because the change in potential due to their motion vanishes on other sites in the crystal in this approximation. Self-consistent calculations⁴ that used calculated deformation potentials to estimate the interaction found that these ions do indeed give substantial contributions to the electron-phonon coupling. Ionic contributions to coupling have been stressed by other authors as well, particularly Jarlborg,¹³ Barišić and co-workers,¹⁴ and Zehyer.¹⁵ Jarlborg has emphasized the importance of charge redistribution in $\text{La}_{2-x}\text{Sr}_x\text{CuO}_4$ due to atomic displacements. He performed self-consistent calculations of both in-plane and axial oxygen breathing mode displacements, reporting charge redistributions as large as ~ 0.4 electrons/a.u. of O_{xy} or O_z displacements. He also found that these charge redistributions lead to important on-site shifts in the spherical part of the potential (as discussed above), which are screened out in conventional, high density-of-state superconductors.

Thus it is necessary to go beyond simple rigid-ion treatments of the electron-phonon coupling. In this paper we employ an *ab initio* approach¹⁶ that makes a minimum of assumptions and that is based on the density functional method. We find nearly harmonic potential surfaces for all the modes discussed here, but anharmonicity would cause these modes to couple. Although there is evidence for anharmonicity both experimentally^{17,18} and theoretically,^{4,19,20} this is neglected in the present calculations. In addition, the density functional eigenvalues and wave functions are assumed to provide a good approximation of the quasiparticle states near E_F , and the adiabatic approximation is assumed to be valid. The substitution of Sr or Ba for La is described by the rigid-band approximation so that the system is perfectly periodic, and all other effects of alloying are neglected in the present calculations. Although there are similar trends in the variation of T_c upon doping with Sr or Ba there are also important differences in the maximum value T_c and other properties. The calculations presented here cannot directly shed light on these other effects of alloying.

Regarding the quality of the eigenvalues and wave functions, the very fact that total energy calculations yield phonon frequencies in good agreement with experiment is one confirmation of the applicability of the local density functional approximation (LDA) to these materials.^{4,19,21} A more direct test of the LDA band structure

is provided by the recent mapping out of the Fermi surface in HTSC by various experimental probes.^{22,23} Angle-resolved photoemission spectroscopy (ARPES) and inverse photoemission spectroscopy (ARIPES) show bands crossing E_F at points in the Brillouin zone in excellent agreement with that predicted by the LDA calculations.^{2,24-26} In interpreting ARPES and ARIPES data, the assumption is often made that the dispersion along the k_z direction is negligible. The three-dimensional character of the band structure in HTSC (and in particular $\text{YBa}_2\text{Cu}_3\text{O}_7$) was emphasized recently.²⁷ The planar and chain derived electronic states hybridize via the out-of-plane oxygen atom, and there is significant c -axis dispersion for some bands. This leads to effective broadening of parts of the Fermi surface when projected into the x - y plane as is done in photoemission experiments. While there is some disagreement over the interpretation of some aspects of these photoemission experiments,²⁸ the experiments generally agree with the Fermi surface predictions of LDA band-structure calculations.² This agreement is consistent with a normal Fermi-liquid picture of the HTSC above T_c .²

While the Fermi surface crossings are predicted well by the LDA bands, the dispersion tends to be steeper than experiment, similar to conventional transition metals. Another possible objection to using the LDA approach is that it does not correctly yield an insulating state for the undoped compound, which displays antiferromagnetic insulating behavior for $x=0$. While this is a deficiency of the LDA for the undoped compound, it does not invalidate its use in the metallic phases, which, as mentioned, are not to be regarded as doped Mott insulators (despite the apparent paradox this wording suggests). There is evidence both from recent Hubbard model calculations²⁹ and photoemission measurements³⁰⁻³⁴ that as the insulating state is doped, additional states fill in the gap region between the valence and conduction bands. In the metallic regime, the LDA description is at least qualitatively correct and, as discussed above, gives an accurate account of the Fermi-surface topology. It is certainly reasonable to proceed on the assumption that the LDA bands and wave functions provide a good approximation of the quasiparticle carrier states near E_F .

II. FORMALISM

The calculational method used here is based on the fact that the electron-phonon coupling constant λ can be expressed as an average over all phonon modes,³⁵

$$\lambda = \frac{1}{Np} \sum_{q,v} \lambda_{q,v}, \quad (1)$$

where $p=3n$ is the number of phonon branches (where n is the number of atoms in the primitive unit cell), N is the number of primitive unit cells, and the contribution $\lambda_{q,v}$ from a single mode of wave vector q , and branch v is related to the electron-phonon-induced linewidth $\gamma_{q,v}$ (half-width at half-maximum) by

$$\lambda_{q,v} = \frac{p\gamma_{q,v}}{\pi\rho(E_F)\hbar\omega_{q,v}^2}. \quad (2)$$

Here $\omega_{q,v}$ is the phonon frequency and $\rho(E_F)$ is the density of states per spin in each unit cell at the Fermi energy. The linewidth, $\gamma_{q,v}$, is given by³⁵

$$\gamma_{q,v} = 2\pi\omega_{q,v} \frac{1}{N} \sum_{nn'\mathbf{k}} |M_{n,\mathbf{k};n',\mathbf{k}-\mathbf{q}}^v|^2 \left[\frac{[f(E_{n,\mathbf{k}}) - f(E_{n,\mathbf{k}} + \hbar\omega_{q,v})]}{\hbar\omega_{q,v}} \right] \delta(E_{n',\mathbf{k}-\mathbf{q}} - E_{n,\mathbf{k}} - \hbar\omega_{q,v}), \quad (3)$$

where E_{nk} is an eigenvalue (for band n and Bloch momentum k) measured with respect to the Fermi energy, and f is the Fermi factor. Usually, the expression involving Fermi factors, $[f(E_k) - f(E_{k+q} + \omega_q)]/\omega_q$, is replaced by $\delta(E_k)$. We have found that this approximation is not satisfactory in $\text{La}_{2-x}\text{M}_x\text{CuO}_4$ due to the combination of high-frequency modes and the quasi-two-dimensional band structure, which is discussed further below. In what follows, it will be convenient to separate the expression for the linewidth into two factors, one that depends on the matrix element and a factor that describes the amount of phase space available for scattering on the Fermi surface via phonons with wave vector q :

$$\gamma_{q,v} = (2\pi\omega_{q,v}) \langle M^2(\mathbf{q}, \nu) \rangle \xi(\mathbf{q}, \omega_{q,v}), \quad (4)$$

where

$$\begin{aligned} \langle M^2(\mathbf{q}, \nu) \rangle &= \frac{\sum_{nn'\mathbf{k}} |M_{n,\mathbf{k};n',\mathbf{k}-\mathbf{q}}^v|^2 \left[\frac{[f(E_{n,\mathbf{k}}) - f(E_{n,\mathbf{k}} + \hbar\omega_{q,v})]}{\hbar\omega_{q,v}} \right] \delta(E_{n',\mathbf{k}-\mathbf{q}} - E_{n,\mathbf{k}} - \hbar\omega_{q,v})}{\sum_{nn'\mathbf{k}} \left[\frac{[f(E_{n,\mathbf{k}}) - f(E_{n,\mathbf{k}} + \hbar\omega_{q,v})]}{\hbar\omega_{q,v}} \right] \delta(E_{n',\mathbf{k}-\mathbf{q}} - E_{n,\mathbf{k}} - \hbar\omega_{q,v})} \\ &\approx \frac{\sum_{nn'\mathbf{k}} |M_{n,\mathbf{k};n',\mathbf{k}-\mathbf{q}}^v|^2 \delta(E_{n,\mathbf{k}}) \delta(E_{n',\mathbf{k}-\mathbf{q}})}{\sum_{nn'\mathbf{k}} \delta(E_{n,\mathbf{k}}) \delta(E_{n',\mathbf{k}-\mathbf{q}})} \end{aligned} \quad (5)$$

and

$$\xi(\mathbf{q}, \omega_{q,v}) = \frac{1}{N} \sum_{nn'\mathbf{k}} \left[\frac{[f(E_{n,\mathbf{k}}) - f(E_{n,\mathbf{k}} + \hbar\omega_{q,v})]}{\hbar\omega_{q,v}} \right] \delta(E_{n',\mathbf{k}-\mathbf{q}} - E_{n,\mathbf{k}} - \hbar\omega_{q,v}). \quad (6)$$

Note that in the expression for the Fermi-surface-averaged matrix elements in Eq. (5), the Fermi-function factors in the numerator and denominator, $[f(E_k) - f(E_{k+q} + \omega_q)]/\omega_q$, have been replaced by $\delta(E_k)$. Numerical tests for $\text{La}_{2-x}\text{M}_x\text{CuO}_4$ have shown that this replacement is less sensitive than in $\xi(q, \omega)$ itself, however, since the same approximation is made in both the numerator and in the denominator of Eq. (5).

Finally, the electron-phonon matrix element is given by

$$M_{n,\mathbf{k};n',\mathbf{k}'}^v = \sum_{\alpha} \left[\frac{\hbar}{2M_{\alpha}\omega_{\mathbf{k}-\mathbf{k}',v}} \right]^{1/2} \left\langle n', \mathbf{k}' \left| \boldsymbol{\varepsilon}_{v,\alpha}(\mathbf{k}-\mathbf{k}') \cdot \frac{\partial V}{\partial \boldsymbol{\tau}_{\alpha}} \right| n, \mathbf{k} \right\rangle, \quad (7)$$

where $\boldsymbol{\varepsilon}_{v,\alpha}(\mathbf{k}-\mathbf{k}')$ is a phonon eigenvector and M_{α} is the mass of the α th ion in the primitive unit cell. The determination of the screened change in the potential $\partial V/\partial \boldsymbol{\tau}$ due to moving a single atom is one of the most difficult aspects of the problem. Consequently, most previous calculations have used some form of rigid-ion approximation, which constrains the electron-phonon interaction to be local.

A more general treatment of this problem¹⁶ determines the change in the screened (i.e., self-consistent or LDA) potential using frozen-phonon supercell calculations. In this approach the matrix elements of $\partial V/\partial \boldsymbol{\tau}$ are determined from the finite difference potential, $\Delta V_{q,v}$, which is the change in self-consistent potential corresponding to the frozen-in phonon,

$$\Delta V_{q,v}(\mathbf{r}) = V[\{\mathbf{R} + \boldsymbol{\tau}_{\alpha} + \Delta \boldsymbol{\tau}_{\alpha,q,v}(\mathbf{R})\}] - V[\{\mathbf{R} + \boldsymbol{\tau}_{\alpha}\}], \quad (8)$$

$$\Delta V_{q,v}(\mathbf{r}) \approx \sum_{\mathbf{R},\alpha} \Delta \boldsymbol{\tau}_{\alpha,q,v}(\mathbf{R}) \cdot \frac{\partial V(\mathbf{r}-\mathbf{R})}{\partial \boldsymbol{\tau}_{\alpha}},$$

where \mathbf{R} is a direct lattice vector, $\boldsymbol{\tau}_{\alpha}$ is the position vector of the α th atom in the unit cell, and the frozen-in atomic displacements of the phonon, $\Delta \boldsymbol{\tau}_{\alpha,q,v}(\mathbf{R})$, are given by

$$\Delta \boldsymbol{\tau}_{\alpha,q,v}(\mathbf{R}) = \Delta u_{q,v} \left[\frac{\hbar}{2M_{\alpha}\omega_{q,v}} \right]^{1/2} \text{Re}[\boldsymbol{\varepsilon}_{v,\alpha}(\mathbf{q}) e^{i\mathbf{q}\cdot\mathbf{R}}], \quad (9)$$

$$\sum_{\alpha=1}^n \boldsymbol{\varepsilon}_{v,\alpha}(\mathbf{q})^* \cdot \boldsymbol{\varepsilon}_{v,\alpha}(\mathbf{q}) = \delta_{v,v}.$$

The actual magnitudes of the ionic displacements in the supercell calculation are controlled by the dimensionless amplitude, $\Delta u_{q,v}$. Alternatively, this amplitude can be expressed in terms of the frozen-in atomic displacements, $\Delta \boldsymbol{\tau}_{\alpha}$:

$$\begin{aligned} (\Delta u_{q,v})^2 &= f(\mathbf{q}) \frac{2M\omega_{q,v}}{\hbar} \left[\frac{1}{MN} \sum_{\alpha,\mathbf{R}} M_{\alpha} \Delta \tau_{\alpha,q,v}^2(\mathbf{R}) \right] \\ &= f(\mathbf{q}) \frac{2M\omega_{q,v}}{\hbar} (\Delta \tau_{\text{rms}})^2, \end{aligned} \quad (10)$$

where M is the total mass in the unit cell, and $f(q)$ is equal to 1 if $q = G/2$ and equal to 2 otherwise, and G is a reciprocal lattice vector. Substituting Eq. (9) into Eq. (8) and using Eq. (7), the matrix elements of $\Delta V_{q,v}/\Delta \tau_{\text{rms}}$ are then given by

$$\left(\frac{\hbar}{2M\omega_{q,v}} \right) \left| \left\langle n', \mathbf{k}' \left| \frac{\Delta V_{q,v}}{\Delta \tau_{\text{rms}}} \right| n, \mathbf{k} \right\rangle \right|^2 = |M_{n,k;n',k'}|^2 \begin{cases} \frac{1}{2}(\delta_{\mathbf{k}',\mathbf{k}-\mathbf{q}} + \delta_{\mathbf{k}',\mathbf{k}+\mathbf{q}}) ; & \mathbf{q} \neq \mathbf{0}; \mathbf{q} \neq \mathbf{G}/2, \\ \delta_{\mathbf{k}',\mathbf{k}-\mathbf{q}} ; & \mathbf{q} = \mathbf{0}; \mathbf{q} = \mathbf{G}/2. \end{cases} \quad (11)$$

Since real displacements of the form given by Eq. (9) are used, the matrix elements of $\Delta V_{q,v}/\Delta \tau_{\text{rms}}$ contribute to $q = k' - k$ and to $-q$ (and these q values are the same if q equals zero or half of a reciprocal lattice vector, G). The matrix elements of $\Delta V_{q,v}/\Delta \tau_{\text{rms}}$ in Eq. (11) are evaluated using the unperturbed wave functions, $|nk\rangle$, calculated in the q -commensurate supercell with the atoms at their ideal positions. Evaluating the matrix element in this supercell results in the simplification¹⁶ that $\mathbf{k}' = \mathbf{k} - \mathbf{q} = \mathbf{k}$ in Eq. (3), since \mathbf{q} is a reciprocal lattice vector in the supercell. Thus the matrix element in Eqs. (3)–(5) is diagonal in \mathbf{k} , with $n \neq n'$. As discussed below, however, it is still convenient to calculate $\xi(q, \omega)$ in Eq. (6) in the primitive Brillouin zone.

There are some drawbacks to this approach. A sufficiently large number of modes must be sampled in the Brillouin zone to get a good estimate of the overall coupling strength λ . However, each mode that is studied requires a separate frozen phonon calculation. For small values of the phonon wave vector q this requires very large supercells and is prohibitive except when applying this method to systems containing only a small number of atoms. In principle, one can surmount these difficulties by using linear response theory,³⁶ doing away with the need for a supercell calculation. Using supercells, however, one must settle for a rather coarse sampling of q . On the other hand, the electron-phonon induced linewidth is automatically obtained for each phonon mode studied, and this can be directly compared with experiment.

III. NUMERICAL IMPLEMENTATION

If the electron wave functions and potentials can be expanded in plane waves as in the pseudopotential method, the calculation of the change in the LDA potential is given simply by an arithmetic difference of Fourier coefficients.¹⁶ A plane wave basis, however, is not practical for the HTSC because of the presence of copper and oxygen atoms, and although the use of the LAPW method in the supercell approach described above is straightforward, some additional work is required to obtain the change in the LDA potential in a form that is convenient for computing the matrix elements. In the LAPW method¹⁰ a dual representation is used for all the relevant quantities. Space is partitioned into two regions, nonoverlapping [muffin-tin (MT)] spheres centered on each atom, and the remaining interstitial region. Within the spheres the basis functions, charge density, and potential are expanded in terms of numerical radial functions multiplied by spherical harmonics. In the interstitial region these quantities are all expanded in plane waves. The dual representation makes it more difficult to compute the electron-phonon matrix elements. Although the same unit cell (i.e., the phonon-commensurate supercell) is used to calculate the potential for the undistorted atomic configuration as well as for the distorted

configuration (corresponding to a finite amplitude frozen-in-phonon, as described above), the interstitial region is slightly different for the two geometries, since one or more of the atoms is displaced from its equilibrium position. In order to calculate the matrix element, the difference in potentials $\Delta V_{q,v}$ must be evaluated and represented with respect to the undistorted MT spheres and interstitial region.

In the LAPW dual representation, the potential is represented as

$$V(\mathbf{r}) = V_{\text{PW}}(\mathbf{r})\theta_I(\mathbf{r}) + V_{\text{MT}}(\mathbf{r})\theta_{\text{MT}}(\mathbf{r}), \quad (12)$$

where θ_I and θ_{MT} are equal to one in the interstitial and MT regions, respectively, and zero otherwise, V_{PW} is the plane-wave representation of the potential, and V_{MT} is the muffin-tin representation of the potential. The potential in the LAPW method that we employ is continuous, and the step functions simply denote that different representations are used in the muffin-tin and interstitial regions. It is convenient to rewrite this as

$$V(\mathbf{r}) = V_{\text{PW}}(\mathbf{r}) + V_{s,\text{MT}}(\mathbf{r})\theta_{\text{MT}}(\mathbf{r}), \quad (13)$$

where $V_{s,\text{MT}} = V_{\text{MT}} - V_{\text{PW}}$, i.e., V_{PW} is now used everywhere in the unit cell and subtracted out again in the MT regions, using the spherical harmonic representation. $V_{s,\text{MT}}$ has the desirable property that it smoothly goes to zero at the MT sphere surface. The difference between the distorted and undistorted potentials is then written as

$$\Delta V(\mathbf{r}) = [V_{\text{PW}}(\mathbf{r}) - V_{\text{PW}}^{(0)}(\mathbf{r})] + [V_{s,\text{MT}}(\mathbf{r} + \Delta \tau_\alpha) - V_{s,\text{MT}}^{(0)}(\mathbf{r})]\theta_{\text{MT}}(\mathbf{r}). \quad (14)$$

The first term is a simple difference of plane-wave coefficients, since the plane-wave terms now extend over the entire unit cell (the same for both geometries). The second term requires more care, but its treatment is now simplified because $V_{s,\text{MT}}$ vanishes on the MT sphere surface, avoiding the necessity of dealing with surface terms. The next step is to decompose $V_{s,\text{MT}}$ into a rigid-ion-like term and a deformation or self-consistent-field (SCF) term inside the MT spheres, by writing

$$V_{s,\text{MT}}(\mathbf{r} + \Delta \tau_\alpha) = V_{s,\text{MT}}^{(0)}(\mathbf{r} + \Delta \tau_\alpha) + \Delta V_{\text{SCF},\text{MT}}(\mathbf{r} + \Delta \tau_\alpha). \quad (15)$$

Since the self-consistency term $\Delta V_{\text{SCF},\text{MT}}$ is already first order in the atomic displacement, $\Delta \tau_\alpha$, this term can simply be used on the undistorted MT sphere position, i.e., $\Delta V_{\text{SCF}}(\mathbf{r} + \Delta \tau_\alpha) = \Delta V_{\text{SCF}}(\mathbf{r}) + \mathcal{O}(\Delta \tau_\alpha^2)$. In order to avoid numerical difficulties in handling the nuclear singularity in the rigid-ion part, the exact first-order expression can be used to express the rigid-ion term. The final expression for $\Delta V_{q,v}$ can then be written as

$$\Delta V_{q,v}(\mathbf{r}) = [V_{PW}(\mathbf{r}) - V_{PW}^{(0)}(\mathbf{r})] + \nabla V_{s,MT}^{(0)}(\mathbf{r}) \cdot \Delta \tau_{\alpha} + \Delta V_{SCF,MT}(\mathbf{r}). \quad (16)$$

The rigid-ion term can be evaluated quasianalytically in terms of $V_{s,MT}^{(0)}$ and its radial derivative times appropriate spherical harmonics combinations, and this is done not

only for the spherical part of $V_{s,MT}^{(0)}$ but for all the non-spherical terms as well. Finally, $\Delta V_{q,v}$ is once again represented in the standard LAPW dual representation, and the matrix element, Eq. (11), is evaluated.

Substituting (11) into (5) and using (2), (4), and (6) we arrive at the following expression for $\lambda_{q,v}$:

$$\lambda_{q,v} = \left[\frac{p}{M \omega_{q,v}^2 \rho(E_F)} \right] \left[\frac{\sum_{n \neq n'; k} \left| \langle n', \mathbf{k} | \frac{\Delta V_{q,v}}{\Delta \tau_{rms}} | n, \mathbf{k} \rangle \right|^2 \delta(E_{n,k}) \delta(E_{n',k})}{\sum_{n \neq n'; k} \delta(E_{n,k}) \delta(E_{n',k})} \right] \xi(\mathbf{q}, \omega_{q,v}),$$

$$= \left[\frac{p}{M \omega_{q,v}^2 \rho(E_F)} \right] \left\langle \left\langle \left[\frac{\Delta V_{q,v}}{\Delta \tau_{rms}} \right]^2 \right\rangle \right\rangle \xi(\mathbf{q}, \omega_{q,v}). \quad (17)$$

where the restriction $n \neq n'$ is required in the supercell.¹⁶ An approximation of the contribution of an entire phonon branch to the electron phonon coupling constant, λ_v ,

$$\lambda = \frac{1}{p} \sum_v \lambda_v \quad (18)$$

can be obtained from (17) by integrating over q and neglecting the q dependence of $\Delta V_{q,v}$ and $\omega_{q,v}$:

$$\lambda_v \approx \lambda_{v,avg} = \left[\frac{\rho(E_F) p}{M \omega_v^2} \right] \left\langle \left\langle \left[\frac{\Delta V_v}{\Delta \tau_{rms}} \right]^2 \right\rangle \right\rangle, \quad (19)$$

having used the fact that the integral over the Brillouin zone of $\xi(q, \omega)$ is approximately equal to $\rho^2(E_F)$ to obtain the estimate, $\lambda_{v,avg}$.

In a test of the method for Al, the delta functions in Eq. (17) [including the delta functions in $\xi(q, \omega)$] were replaced by normalized Gaussians, and $\lambda_{q,v}$ evaluated as a discrete sum over a uniform sampling of k points in the supercell Brillouin zone as was done in Ref. 16. Very good agreement with the results of Dacorogna *et al.*¹⁶ for selected q values were obtained.³⁷ Similar tests³⁷ for selected phonon modes in niobium yielded good agreement with the results of rigid-ion calculations of Butler *et al.*³⁸ and with the experimentally measured phonon linewidths of Wakabayashi.³⁹

Using Gaussian broadening in place of the delta functions, however, was found to be inadequate in $\text{La}_{2-x}\text{M}_x\text{CuO}_4$ ($M = \text{Sr}$ or Ba), the results being too sensitive to the number of k points used and the size of the broadening. The reason for this sensitivity is revealed from inspection of Eqs. (3)–(6), especially in the $\omega \rightarrow 0$ limit. While $\langle M^2(q, v) \rangle$ depends on the matrix elements but not too sensitively on the k -point sampling, $\xi(q, \omega)$ is independent of the matrix elements but quite sensitive to the k -point sampling, since, in the limit that ω goes to zero, $\xi(q, \omega)$ is a Fermi-surface line integral. Although it is sufficiently accurate for $\langle M^2(q, v) \rangle$, the replacement of the delta functions in $\xi(q, \omega)$ by normalized Gaussians leads to a poor representation of ξ , and an alternative method of calculation must be used. It is useful to consider the related quantity $\xi'(q, \omega, E)$,

$$\xi'(q, \omega, E) = \frac{1}{N} \sum_{nn'k} \delta(E_{n,k} + \hbar\omega - E) \delta(E_{n',k-q} - E_{n,k} - \hbar\omega), \quad (20)$$

whose integral is just $\xi(q, \omega)$:

$$\xi(q, \omega) = \frac{1}{\hbar\omega} \int_0^{\hbar\omega} \xi'(q, \omega, E) dE. \quad (21)$$

$\xi(q, \omega)$ is related to the generalized susceptibility^{40,41} χ by $\xi(q, \omega) = (\pi\omega)^{-1} \text{Im}\chi(q, \omega)$, and describes the phase space available for scattering quasiparticles within $\hbar\omega$ of E_F through wave vector q from k to $k+q$.⁴² This is a very anisotropic quantity in $\text{La}_{2-x}\text{M}_x\text{CuO}_4$ due to strong Fermi-surface nesting all along the (1,1,0) line and a nesting of van Hove singularities [located at $k = (1/2, 0, 0)\pi/a$] for q near the X point, $(1, 1, 0)\pi/a$. The Fermi surface for $x=0.15$ is shown in Fig. 1. Previously, $\xi'(q, 0, 0)$ was found⁴² to have a strong q dependence, and there is a large peak at the X point due to strong Fermi-surface nesting^{40,41} between slightly smeared van Hove singularities, as seen in Fig. 2(a) [Fig. 2(b) displays the related function, $\xi_{tr}(q, 0, 0)$, discussed further below]. In addition to this expected peak, however, a strong enhancement is found all along the $\langle 110 \rangle$ direction arising from scattering along the flat sides of the Fermi surface seen in Fig. 1.

Concerning the electron-phonon interaction, this indicates much larger phonon linewidths due to electron-hole creation for phonons along this direction than elsewhere in the Brillouin zone and hence much larger contributions to λ from this direction, assuming that the q dependence of the matrix element $\langle M^2(q, v) \rangle$ does not counteract this. This is discussed further below. As mentioned, it is usual to simply replace $\xi(q, \omega)$ by its $\omega=0$ value, $\xi'(q, 0, 0)$. Because of the quasi-two-dimensional band structure and the van Hove singularity, however, this approximation is not satisfactory here especially for wave vectors near X . This is illustrated in Fig. 2(c) which shows $\xi(q, \omega)$ plotted as a function of q_y along $\langle 1, q_y, 0 \rangle \pi/a$ for several values of ω . At fixed q , $\xi(q, \omega)$ is generally larger for smaller ω . The effect is especially

dramatic at the X point.

We calculated $\xi(q, \omega)$ by numerically integrating Eq. (21). $\xi'(q, \omega, E)$ was determined at about 16 different E 's for each ω using the linear analytic tetrahedron method.⁴³ Since $\xi'(q, \omega, E)$ does not depend on the matrix elements, it can be more efficiently evaluated in the primitive Brillouin zone (rather than usual the supercell geometry) as a function of the phonon wave vector q and the frequency arguments. To do this, the energy bands were first calculated at 135 k points in the primitive irreducible Brillouin zone, and a spline fit⁴⁴ to symmetrized plane waves was then used to generate about 10^6 points in the Brillouin zone, which are then used in the tetrahedron method. (A rigid-band approximation is used to determine the Fermi energy corresponding to a concentration $x=0.15$.) Even with this many points the line integral in Eq. (20) is a rather sensitive quantity to determine. For example, $\xi'(q, 0, 0)$ can vary by about 40% as q varies by as little as $0.02 \pi/a$ near the X point. The sensitivity is reduced for nonzero ω , and we estimate the integrated quantity $\xi(q, \omega)$ to be accurate to at least 10%.

Having calculated $\xi(q, \omega, \nu)$, the averaged matrix element $\langle M^2(q, \nu) \rangle$ in Eqs. (4) and (5) is then calculated for the zone-boundary phonons in the following manner. The band structure for the *undistorted supercell* is first calculated at a large number (70) of k points in the irre-

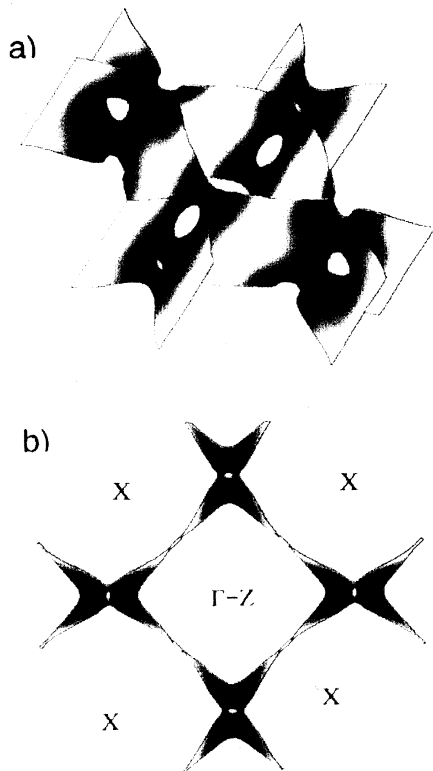


FIG. 1. Two views of the Fermi surface for $\text{La}_{1.85}\text{M}_{0.15}\text{CuO}_4$. (a) The shaded areas indicate low-velocity regions near the van Hove singularities at the corners. (b) The Γ - Z axis is perpendicular to the page in this view, which indicates the degree of smearing of the van Hove singularities due to k_z dispersion.

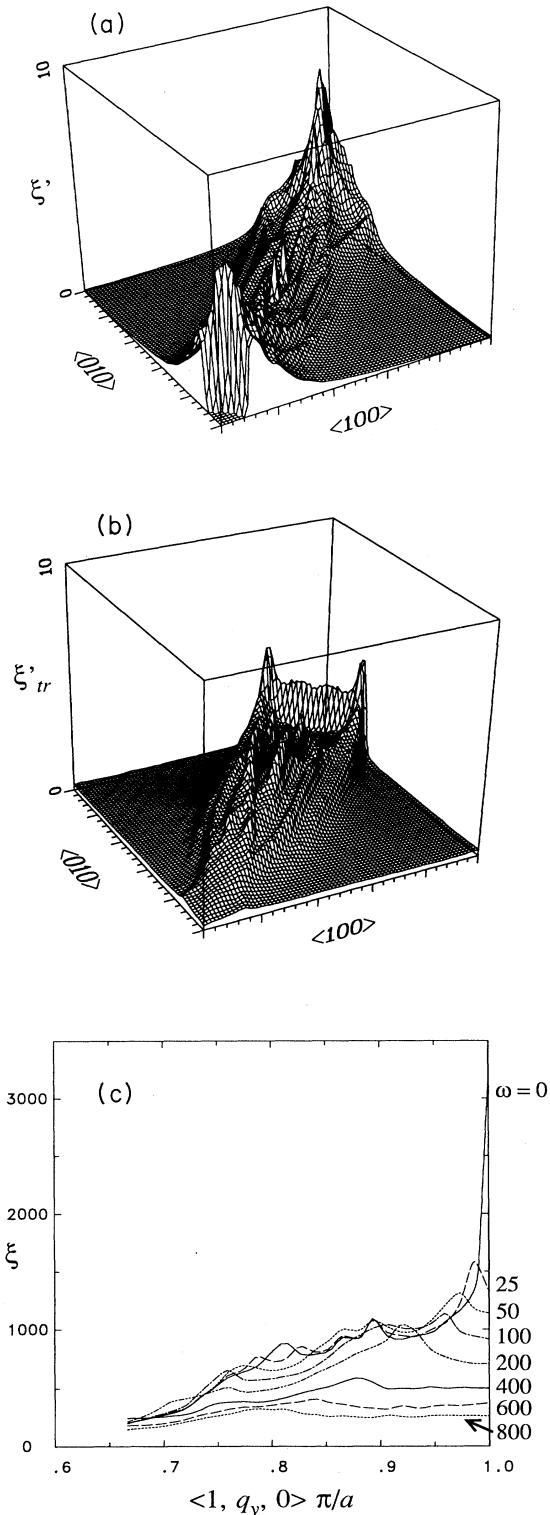


FIG. 2. Three-dimensional plot of the Fermi-surface phase factors (a) $\xi'(q, 0, 0)$ and (b) $\xi'_{tr}(q, 0, 0)$ for $\text{La}_{1.85}\text{M}_{0.15}\text{CuO}_4$ as a function of wave vectors q in the x - y plane. Shown here are these functions averaged over values of $q_z=0, \pi/c, \text{ and } 2\pi/c$. The $q \rightarrow 0$ divergence in $\xi'(q, 0, 0)$ is cut off for clarity. (c) $\xi(q, \omega)$ along $q = \langle 1, q_y, 0 \rangle \pi/a$ for several values of ω .

ducible Brillouin zone. A spline fit (as described above) is then used to generate a very dense uniform sampling of k points throughout the zone. A subset of these k points is then identified for which two bands are equal to E_F (to within about ± 5 mRy, roughly equal to the maximum phonon energy); this degeneracy is due to folding of the bands into the smaller Brillouin zone of the supercell. For example, one band crosses E_F in the primitive Brillouin zone, so there are two in the $q=(\pi/a, \pi/a, 0)$ supercell, and these are degenerate on the points representing the line integral in Eq. (5). There were 33 k points in this subset for the X -point phonons. The band eigenvalues were then calculated at these k points and used to evaluate the line integral average, $\langle M^2(q, \nu) \rangle$, in Eq. (5), with the delta functions safely replaced by Gaussians. The resulting average matrix element is less sensitive to the number of k points and the magnitude of the Gaussian broadening, as desired. By contrast, if $\xi(q, \omega)$ were calculated in this manner, it would be very sensitive to these quantities. Finally, we used the experimental structure for La_2CuO_4 as determined by Longo and Raccach,⁴⁵ and the value $\rho(E_F)=14.2$ (Ry-cell-spin)⁻¹ was also determined using the tetrahedron method.

IV. RESULTS AND DISCUSSION

A. Matrix elements and mode coupling strengths

Results for $\langle (\Delta V/\Delta\tau_{\text{rms}})^2 \rangle$, $\xi(q, \omega)$, $\lambda_{q, \nu}$, $\lambda_{\nu, \text{avg}}$, and $\gamma_{q, \nu}$ of selected phonons are presented in Tables I–VIII. X -point phonons in $\text{La}_{2-x}\text{M}_x\text{CuO}_4$ are given in Tables I and II. (The X -point eigenmode frequencies in Table I of Ref. 19 are incorrect due to an error in converting units. The corrected values are given here. The symmetry mode frequencies and the eigenvectors were unaffected by this transient error.) All fully symmetric (A_g) modes, i.e., having the symmetry of the oxygen planar-breathing mode (see also Ref. 19), as well as three modes having B_{3g} symmetry are examined. These two symmetries were chosen for study partially because both are compatible with tetragonal Σ_1 symmetry, which experiment has shown to be particularly interesting. The eigenvectors

for the A_g (Table III) and the B_{3g} (Table IV) modes are also reproduced here. The 137- and 263-cm⁻¹ A_g modes consist primarily of La and O_z axial displacements, respectively. The 417-cm⁻¹ mode has planar oxygen atoms vibrating in-plane and perpendicular to the Cu—O bond (“scissors” motion), and the 642-cm⁻¹ “breathing” mode has planar oxygens moving toward or away from the Cu atoms. In Table II, the 329-cm⁻¹ mode is the Cu motion along (the orthorhombic) x , while the 65-cm⁻¹ and 282-cm⁻¹ modes involve La and O_z moving together or in opposite directions along x , respectively.

The X -point frequencies are compared with experiment^{46–49} in Table V. Where a range of experimental values is quoted for Ref. 46, there is a noticeable doping dependence. Also there are two experimental modes in Ref. 46 in the range 293–310, and the symmetry types label only the theoretical frequencies. The experimental range labeled “extra modes” denote regions in the Brillouin zone near X where there is additional observed intensity; these had been related to “extra modes” due to strong anharmonic electron-phonon coupling, but are now attributed by Pintschovius *et al.*⁴⁶ to remnants of branches of the orthorhombic phase. The fact that these are seen is attributed to strong anharmonicity. The effects of anharmonicity are discussed further below.

Table VI presents results for the axial apex-oxygen (O_z) and lanthanum modes at the $q=(0, 0, 2\pi/c)$ zone boundary (Z). The eigenvectors for these Z -point modes are given in Table VII. Table VIII presents matrix elements for these modes at $q=0$ (Γ). Results for La obtained using the RMT approximation are also shown here. By RMT, we mean that only the rigid-ion-like term in Eq. (16) is retained. The standard formulas for the RMT approximation implicitly include contributions from all phonon modes, and the results are expressed in terms of scattering phase shifts. Furthermore, cubic symmetry is usually assumed to simplify the equations. In the present numerical evaluation no assumptions about symmetry are made.

The small matrix elements using the RMT approximation compared to the large values computed using the full theory illustrate the importance of the unusual long-

TABLE I. Frequencies, electron-phonon matrix elements, phase space factor, $\xi(q, \omega)$, coupling strength, $\lambda_{q, \nu}$, linewidths $\gamma_{q, \nu}$, and Brillouin zone averaged coupling strengths, $\lambda_{\nu, \text{avg}}$, for fully symmetric (A_g) X -point modes for concentration $x=0.15$.

	$\omega_{q, \nu}$ (cm ⁻¹)	$\langle (\Delta V/\Delta\tau_{\text{rms}})^2 \rangle$ [(eV/a.u.) ²]	$\xi(q, \omega)$ [(Ry cell) ⁻²]	$\lambda_{q, \nu}$	$\gamma_{q, \nu}/\omega_{q, \nu}$	$\lambda_{\nu, \text{avg}}$
Symmetry modes						
La axial	155	0.003	795	0.028	0.00	0.01
O _z axial	339	4.55	552	5.7	0.037	2.08
O quad.	404	0.12	497	0.09	0.001	0.04
O brea.	609	4.53	360	1.15	0.014	0.64
Eigenmodes						
	137	0.66	829	7.6	0.020	1.86
	263	1.24	626	2.9	0.015	0.94
	417	0.28	486	0.21	0.002	0.086
	642	7.64	339	1.6	0.020	0.97

TABLE II. Same as Table I for B_{3g} modes at X .

	$\omega_{q,v}$ (cm^{-1})	$\langle (\Delta V / \Delta \tau_{\text{rms}})^2 \rangle$ [(eV/a.u.) ²]	$\xi(q, \omega)$ [(Ry cell) ⁻²]	$\lambda_{q,v}$	$\gamma_{q,v} / \omega_{q,v}$	$\lambda_{v,\text{avg}}$
Symmetry modes						
La	143	0.030	820	0.31	0.0009	0.075
O _z	258	0.033	633	0.082	0.0004	0.026
Cu	323	0.028	567	0.039	0.0002	0.014
Eigenmodes						
	65	0.036	1053	2.3	0.0029	0.45
	282	0.038	610	0.08	0.0004	0.026
	329	0.016	563	0.02	0.0001	0.008

range Madelung-like couplings that are present in these materials. Such long-range off-site contributions are also important for the O_z modes. For example, the Z-point O_z symmetry mode has approximately equal additive contributions from the O_{xy} atoms as for the on-site O_z contributions. The contributions from the Cu atoms for this mode are about half as large, but are of opposite sign. Falter *et al.*⁵⁰ have predicted that the apex-oxygen breathing mode at the Z point should lead to a large non-local electron-phonon interaction of this type by inducing crystal potential changes of the same sign in the whole CuO plane. As seen in Table VIII the matrix element for the O_z mode at (0,0,2 π /c) is quite large, but it is even larger at $q=(0,0,0)$ where the induced changes in the CuO plane would have opposite signs in their picture.

In the symmetry modes in Tables I and II, the other atoms were kept at their equilibrium positions. This neglects, however, the coupling between displacements of the same symmetry. At the X point in La₂CuO₄, the total energy was calculated as a function of displacement for the four atomic distortions that have a full A_g symmetry of the X point and the three B_{3g} modes. In addition the energy for combinations of these symmetry modes was also calculated in order to obtain the full dynamical matrix of modes of each symmetry type.¹⁹ By diagonalizing the respective dynamical matrices, the eigenvectors and frequencies of all seven modes were obtained, the eigenvectors giving the relative displacements for each mode. These eigenvectors are then used to form the appropriate linear combination of the symmetry mode matrix elements, $\langle (\Delta V / \Delta \tau_{\text{rms}}) \rangle$, to yield the eigenmode matrix element. The eigenvectors are given in Tables III and IV together with the frequencies. The eigenvectors for the Z-point mode are given in Table VII. The relative displacements of the atoms are obtained by dividing the eigenvector coefficients by the square root of the mass.

TABLE III. Eigenvectors for the fully symmetric modes in Table I.

Eigenmodes	La	O _z	O _{xy} quad.	O _{xy} breathing
137	0.95	0.29	0.05	0.07
263	-0.30	0.85	-0.32	-0.31
417	-0.05	0.28	0.94	-0.16
642	-0.03	0.35	0.05	0.94

There are substantial O and Cu displacements in the lower frequency (La) eigenmodes. For example, the La and O_z displacements are nearly the same in the 121- cm^{-1} mode at the Z point. This coupling also raises the frequency of the normal mode consisting mostly of oxygen-planar breathing motion from 609 to 642 cm^{-1} . More importantly it results in substantial hybridization between this high-frequency planar oxygen mode and the lower frequency axial oxygen mode at 263 cm^{-1} . Similar behavior was found for Γ point ($q=0$) modes in YBa₂Cu₃O₇.⁴ In this manner, the strong coupling to O_z motion that is most evident at high frequency is transferred to lower frequencies.

In the normal state, $q=0$ phonons do not couple to the electrons, since energy cannot be conserved: for sufficiently small q optic phonons (specifically, for $q v_k < \omega_q$), if E_k is on the Fermi surface, then $E_k \pm \hbar \omega_{q=0}$ cannot be (barring interband transitions, which do not occur in the high-temperature tetragonal phase of LSCO, since only a single band cross E_F). Thus $\lambda_{q=0,v}$ is strictly zero. However, onset of coupling occurs at phonon wave vectors $q \sim \omega_{q,v} / v_F$, which is a small fraction of the Brillouin zone dimension, where v_F is the Fermi velocity. (Raman measurements of this onset of Landau damping were recently reported by Friedl *et al.*⁹) We have taken the $q=0$ calculated matrix elements (assumed constant for small q) to estimate a branch average, $\lambda_{v,\text{avg}}$, for the corresponding phonon branch. Only symmetry modes were considered for the $q=0$ O_z and La A_g symmetry displacements. Eigenmodes of the two A_g symmetry modes at $q=0$ were previously calculated and the coupling of these symmetry modes was found to be small.¹⁹ We have also estimated the branch contributions from the Z-point and X-point modes.

An overall estimate of λ can then be obtained by averaging all of the values of $\lambda_{v,\text{avg}}$. In averaging these quantities, the three axial-La modes are first averaged to

TABLE IV. Eigenvectors for the B_{3g} modes in Table II.

Eigenmodes	Cu	O _z	La
65	-0.10	0.44	0.89
282	-0.30	-0.87	0.39
329	0.95	-0.23	0.22

TABLE V. Comparison of X -point experimental phonon frequencies with the calculated phonon modes in Tables I and II. All frequencies are in cm^{-1} . Where a range of values is quoted, there is noticeable doping dependence.

Symmetry	Expt.	Calc.
A_{1g}	706, ^a 710, ^b 680 ^c	642
A_{1g}	490 ^a	417
B_{3g}	373 ^a	329
B_{3g}	293–310 ^a	282
A_{1g}	293–310 ^a	263
“extra modes”	253 ^a	
A_{1g}	150–157, ^a 137 ^d	137
B_{3g}	117–120 ^a	65

^aReference 46.

^bReference 47.

^cReference 48.

^dReference 49.

provide an overall estimate for this branch. The same is done with the three axial-O modes. These values and the overall average $\lambda=1.37$ are shown in Table IX. Dominant contributions are seen to come from apex-O and La atoms, due to unusual non-rigid-ion long-range Madelung-like coupling. A value of λ this large easily accounts for T_c in this compound. We use the Allen-Dynes⁵¹ strong-coupling equation for T_c :

$$T_c = f_1 f_2 \frac{\omega_{\log}}{1.20} \exp \left[\frac{-1.04(1+\lambda)}{\lambda - \mu^*(1+0.62\lambda)} \right]. \quad (22)$$

The factors f_1 and f_2 are close to 1 for $\lambda=1.37$, and ω_{\log} is evaluated using

$$\ln(\omega_{\log}) = \frac{1}{\lambda_{\text{avg}} m} \sum_{v=1}^m \lambda_{v,\text{avg}} \ln(\omega_{v,\text{avg}}), \quad (23)$$

$$\lambda_{\text{avg}} = \frac{1}{m} \sum_{v=1}^m \lambda_{v,\text{avg}}.$$

The contributions to ω_{\log} from $m=7$ “branches” are given in Table IX. Using $\omega_{\log}=321 \text{ cm}^{-1}$ obtained in Table IX and $\lambda=1.37$ together with $\mu^*=0.1$, yields $T_c=49 \text{ K}$, which is close to the experimentally observed value. For $\mu^*=0.15$ and 0.2 , $T_c=41$ and 32 K , respectively. The precise value is not especially meaningful considering the sampling of phonon modes that were

used, but is of the right order to account for T_c in this material.

An old question concerns the consistency of large λ 's such as are found here with transport measurements. Gurvitch and Fiory⁵² used early polycrystalline resistivity data to estimate λ for $\text{YBa}_2\text{Cu}_3\text{O}_7$, assuming that λ and λ_{tr} are similar in magnitude as in conventional superconductors. This analysis led to unphysically small mean free paths for the large values of λ_{tr} they derived from the data. Mazin and Dolgov⁵³ have analyzed more recent single-crystal data, using their LDA band-structure calculations for the plasma frequency and mean Fermi velocities to derive a smaller λ_{tr} of about 1.5 and a reasonably large mean free path of 11 \AA at $T=300 \text{ K}$. Zeyher⁵⁴ has also examined the question of phonon-limited resistivity in the high- T_c oxides. He used a screened ionic model to calculate $\lambda_{\text{tr}} \sim 1$ and $\lambda \sim 3$ for $\text{YBa}_2\text{Cu}_3\text{O}_7$. For large λ_{tr} or λ , he found that the small ratio $\lambda_{\text{tr}}/\lambda$ is crucial in obtaining agreement with the experimentally measured slope of the temperature dependence of the resistivity, since for $\lambda_{\text{tr}}=\lambda$, the experimental slope would imply $\lambda \sim 0.2$.⁵⁴

The matrix element for λ_{tr} is weighted by the square of the difference in electron velocities between the state at k and $k+q$ (which accounts for the amount of current lost by the scattering event) so that λ_{tr} can be significantly different from λ . Recent theoretical work for Fermi surfaces like that of $\text{La}_{2-x}\text{M}_x\text{CuO}_4$, which have the strong nesting feature already noted along the $(1,1,0)$ direction, shows that the square of the difference in velocities can be quite anisotropic and may result in a large reduction of λ_{tr} compared to λ .⁵⁵ We have calculated $\xi'_{\text{tr}}(q,0,0)$, shown in Fig. 2(b), which is $\xi'(q,0,0)$ weighted with the above-mentioned square difference of the electron velocities. Unlike $\xi'(q,0,0)$ which is singular at $q=0$, $\xi'_{\text{tr}}(q,0,0)$ goes smoothly to zero. It is largest along the $[1,1,0]$ direction as is $\xi'(q,0,0)$, but more spread out, and it is small right at the X point where $\xi'(q,0,0)$ itself is very large. Both the very large value of $\xi'(q=X,0,0)$ and the small value of $\xi'_{\text{tr}}(q=X,0,0)$ can be accounted for by nesting of van Hove singularities (slightly broadened by k dispersion). The model calculation of Crespi and Cohen⁵⁵ suggests that such behavior, coupled with strong q dependence of matrix elements, can result in λ being significantly larger than λ_{tr} . We are pursuing this question.

TABLE VI. Same as Table I for fully symmetric Z -point modes for concentration $x=0.15$. Rigid-muffin-tin (RMT) values are also given for the lanthanum symmetry mode.

	$\omega_{q,v}$ (cm^{-1})	$\langle (\Delta V / \Delta \tau_{\text{rms}})^2 \rangle$ [(eV/a.u.) ²]	$\xi(q,\omega)$ [(Ry cell) ⁻²]	$\lambda_{q,v}$	$\gamma_{q,v}/\omega_{q,v}$	$\lambda_{v,\text{avg}}$
Symmetry modes						
La	202	0.79	948	4.8	0.02	1.0
La (RMT)	202	0.08	948	0.48	0.00	0.1
O ₂ axial	396	13.9	621	14	0.11	4.7
Eigenmodes						
	121	0.18	1054	3.3	0.01	0.64
	414	14.4	598	13	0.11	4.4

TABLE VII. Eigenvectors for the Z -point modes in Table VI.

Eigenmode	La	O _z
121	0.95	-0.30
414	0.30	0.95

B. Mode linewidths

We turn now to a discussion of the results for the calculated linewidths. While quite small linewidths are found for the three B_{3g} modes at the X point, moderate linewidths are found for the fully symmetry modes at the X point, the largest being $\gamma_{q,v}/\omega_{q,v} \sim 0.02$. This corresponds to $\lambda_{q,v} = 7.6, 2.9,$ and 1.6 for the La, O_z, and breathing modes, respectively. These linewidths may be difficult to detect by neutron scattering. By contrast, the axial-O_z mode at the Z point in Table VI has a very large linewidth of $\gamma_{q,v}/\omega_{q,v} \sim 0.1$ ($\lambda_{q,v} = 13$) and should be easier to observe. An experimental difficulty may be that if there are nonsuperconducting phases present in the sample, they would yield sharp phonon lines, and the broader signal from the superconducting phase may be overlooked as part of the background.

Since the phase space factor $\xi'(q,0,0)$ is so strongly q dependent and peaks at the X point, the total contribution of a given phonon branch to λ may be smaller than implied by the linewidths at the X point. Thus, if one assumes a q -independent matrix element, i.e., $\langle (\Delta V(q)/\Delta\tau_{\text{rms}})^2 \rangle \sim \langle [\Delta V(q=(\pi/a, \pi/a, 0))/\Delta\tau_{\text{rms}}]^2 \rangle$ and neglects dispersion for this phonon branch, the expression in Eq. (19) yields an estimate for this entire branch. This estimate is also made for the other calculated phonon modes and is shown in the respective Tables. For example, as seen from Table I, the 642-cm⁻¹ mode has $\lambda_{v,\text{avg}} = 0.97$ compared to $\lambda_{q,v} = 1.6$. This would tend to lower its contribution to λ , assuming that $\langle (\Delta V(q)/\Delta\tau_{\text{rms}})^2 \rangle$ for this mode does not increase for smaller q .

From Tables VI and VIII, however, it is clear that in

TABLE VIII. Matrix elements and $\lambda_{v,\text{avg}}$ for axial apex-oxygen and lanthanum modes at $q=0$. Rigid-muffin-tin (RMT) values are also given for the lanthanum modes.

	$\omega_{q,v}$ (cm ⁻¹)	$\langle (\Delta V/\Delta\tau_{\text{rms}})^2 \rangle$ [(eV/a.u.) ²]	$\lambda_{v,\text{avg}}$
La (RMT)	224	0.11	0.12
La	224	4.33	4.54
O _z	415	38.3	11.7

fact the matrix elements do increase for smaller q , at least for the axial-La and -O_z modes. For example, the La symmetry-mode matrix element is greatly reduced at the X point in Table I [0.003 (eV/a.u.)²] compared to its values at $q=0$ and $(0,0,2\pi/c)$ in Tables VIII and VI [4.33 and 0.79 (eV/a.u.)², respectively]. Similarly, the axial-O_z symmetry mode is increased at $q=0$ and $(0,0,2\pi/c)$ [38.3 and 13.9 (eV/a.u.)², respectively] compared to its value at the X point [4.55 (eV/a.u.)²] in Table I. Since $\xi(q,\omega)$ is strongly peaked along the $q=(1,1,0)\pi/a$ direction, this suggests that phonon modes along this direction yield the largest contributions to λ . Thus the estimate of λ obtained from sampling points only at X and near $q=0$ (Γ and Z) may not be unreasonable.

C. Character of electron-phonon coupling

The wave functions that contribute to the matrix elements for the X -point modes are antibonding Cu-O states that have about equal weight on the copper and the planar and apex oxygen atoms. The charge density corresponding to the sum over the subset of 33 k points used to determine the average matrix elements at $q=X$ is shown in Figs. 3 and 4 (the total charge is equal to one electron). Individually, the states at these different k points have similar spatial behavior. These states have about equal weight on the O_z as on the O_{xy} atoms (for the charge density displayed in Figs. 3 and 4, there are only 10% less electrons within the O_z muffin-tin spheres than within the O_{xy} spheres). Correspondingly, there is also substantial density of states on the O_z atom (only about

TABLE IX. λ and ω_{log} from 7 "branches." The axial La and O_z values are averages of $\Gamma, Z,$ and X .

Mode	$\omega_{v,\text{avg}}$ (cm ⁻¹)	$\lambda_{v,\text{avg}}$	$\lambda_{v,\text{avg}} \ln(\omega_{v,\text{avg}})$
La-ax (Γ)	224	4.54	24.6
La-ax (Z)	121	0.64	3.1
La-ax (X)	137	1.86	9.2
La-ax avg		2.35	12.3
O _z -ax (Γ)	415	11.7	70.5
O _z -ax (Z)	414	4.40	26.5
O _z -ax (X)	263	0.94	5.24
O _z -ax avg		5.68	34.1
O-quad	417	0.09	0.52
O-br	642	0.97	6.30
La-B _{3g}	65	0.45	1.88
O-B _{3g}	282	0.03	0.17
Cu-B _{3g}	329	0.01	0.06
λ_{avg}		1.37	
ω_{log} (cm ⁻¹)			321

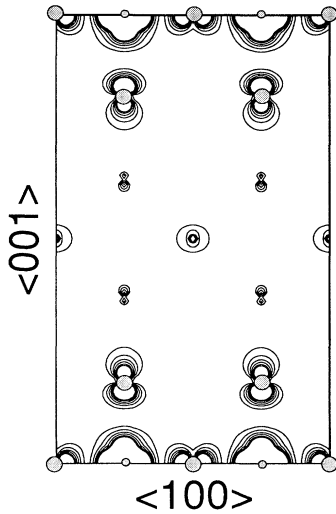


FIG. 3. Charge density contour plot in the x - z plane corresponding to the sum over the subset of 33 k points used to determine the average matrix elements at $q = X$. The small circles locate the copper atoms and the large circles locate the oxygen atoms. The contour levels run from 0.005 to 0.030 in steps of 0.005 electrons/a.u.³

40% less¹² than on the O_{xy} atom). Recent oxygen K - and copper L -edge absorption spectra of Chen *et al.*⁵⁶ confirm this, showing a significant amount of $O\ 2p_z$ character for doping induced holes. However the calculated RMT electron-phonon parameter, $\eta(O_z)$, was previously found to be about an order of magnitude smaller than for the O_{xy} atom.⁵⁷ The principal reason for this is that the oxygen contributions in the RMT all come from $p \rightarrow d$ scattering, and the d density of states on the O_z site (arising from the $l=2$ symmetry combinations of tails of orbitals on neighboring atoms) is about a factor of 6 lower than on the O_{xy} site. Additional factors due to muffin-tin potential differences further reduce the RMT contribu-

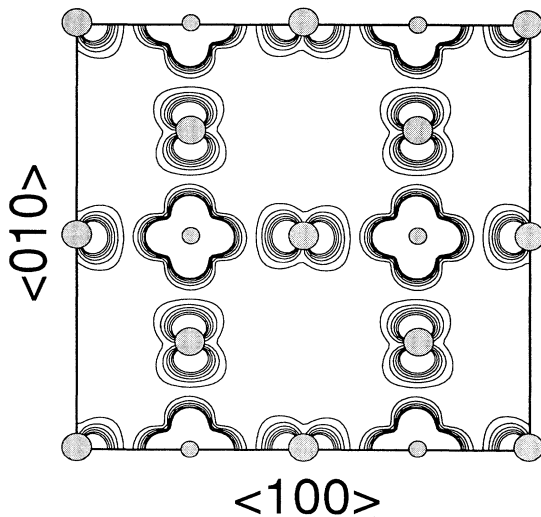


FIG. 4. Same as Fig. 3 but in the x - y (CuO) plane.

tion on the O_z atom. Long-range Madelung-like contributions (discussed above) are large in these materials, however, and result in much stronger coupling than predicted by the RMT approximation which neglects off-site contributions to $\Delta V_{q,v}$.

The self-consistent change in the LDA potential, $\Delta V_{q,v}$, or the 642-cm^{-1} planar-oxygen breathing mode at the X point (Table I) is shown in Fig. 5, and $\Delta V_{q,v}$ for the 417-cm^{-1} planar-oxygen quadrupolar ("scissors") mode at the X point (Table I) is shown in Fig. 6. Examination of the charge density in Figs. 3 and 4 and $\Delta V_{q,v}$ for the quadrupolar mode in Fig. 6 explains why the planar-O quadrupolar mode has such a small linewidth compared to the planar-O breathing mode, since there is poor overlap of the wave functions with ΔV for this mode. By contrast, the planar-O breathing mode Fig. 5 and the apex-O A_g modes overlap strongly with ΔV .

In the RMT approximation, the La modes should not couple at all, since there are no electron states at E_F that have significant weight on the La site. Because long-range Madelung-like interactions are included in this calculation, however, there are strong contributions from La modes. The poor screening in the high-temperature superconductors normal to the Cu-O planes is a novel feature of these materials and is responsible for this unusual behavior. The coupling to La displacements is further enhanced for the X -point eigenmodes by coupling with higher frequency symmetry modes that have larger matrix elements. The relative importance of a mode for T_c is given not simply by $\lambda_{q,v}$, which can be greatly enhanced by low frequencies, but rather by a quantity between $\omega_{q,v}\lambda_{q,v}$ and $\omega_{q,v}^2\lambda_{q,v}$.⁵⁸ Thus, hybridization can play an important role in determining at which frequency the electron-phonon coupling occurs. Furthermore, hy-

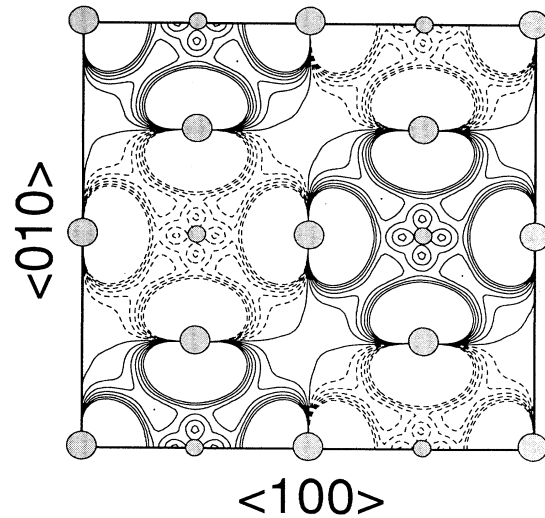


FIG. 5. $\Delta V_{q,v}/\Delta\tau_{rms}$ contour plot for the 642-cm^{-1} planar-oxygen breathing mode at the X point. Negative contour values are represented by dashed lines. The small circles locate the copper atoms and the large circles locate the oxygen atoms. The contour levels run from -1.50 to 1.50 in steps of 0.25 Ry/a.u. ~ 6.5 eV/Å.

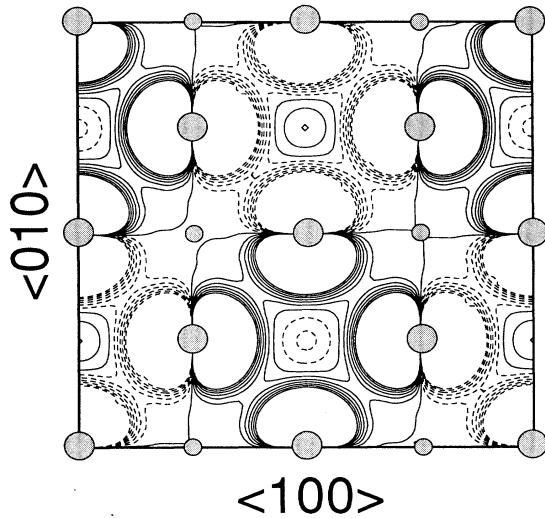


FIG. 6. $\Delta V_{q,v}/\Delta\tau_{rms}$ contour plot for the 417-cm^{-1} planar-oxygen quad. mode at the X point. Negative contour values are represented by dashed lines. The small circles locate the copper atoms and the large circles locate the oxygen atoms. Contour levels are the same as in Fig. 5.

bridization of light-ion and heavy-ion symmetry modes can lower the expected isotope effect for oxygen.¹⁹

D. Questions of anharmonicity

An important element left out of this analysis is the effect of anharmonicity. Several of the modes not considered here are *very anharmonic*, including at least two at the X point that are unstable.^{19,20} Anharmonic modes have also been found in $\text{YBa}_2\text{Cu}_3\text{O}_7$.¹⁹ Of particular interest are the instabilities of X -point tilts of the CuO_6 octahedra that are responsible for the high-temperature tetragonal (HTT) to low-temperature orthorhombic (LTO) structural transition.¹⁹ In addition, Axe *et al.*⁵⁹ established that the previously observed⁶⁰ strong suppression of T_c in $\text{La}_{1.88}\text{Ba}_{0.12}\text{CuO}_4$ near $x=0.12$ is correlated with a further structural phase transition from the LTO structure to a low-temperature tetragonal (LTT) structure. We have reported²⁰ earlier the energy surface in the space spanned by the two degenerate LTO order parameters. An eight-well potential was found with HTT being a local maximum and the LTT structure the absolute minimum, and LTO being a local minimum, which is just the energy surface required to account most easily for the phase diagram of $\text{La}_{1.88}\text{Ba}_{0.12}\text{CuO}_4$. This energy surface is indicative of strongly anharmonic lattice dynamics, especially near the X point, and this may account for what has been seen in the form of “extra modes” (Table V) by Reichardt *et al.*⁶¹

Unlike the case for the LTO phase, where the band structure near E_F is not much changed, the LTT distortion splits the bands at E_F (for E_F corresponding to $x=0.12$ in a rigid-band calculation).²⁰ In the LTO structure, two normal modes arise from the tilt modes.⁶² The high-frequency mode corresponds to tilt amplitude modulations, which our calculations show to have little

effect on the band structure at E_F ,²⁰ and a low-frequency mode that corresponds to changes in tilt direction toward the LTT structure. Recent results by Cohen *et al.*⁶³ show that though the linear electron-phonon coupling for small rotations (relative to the HTT structure) is essentially zero, there is a significant quadratic coupling. For rotations relative to the LTT minima, however, the linear coupling may also become significant.

It is difficult to assess the effect of such anharmonic modes, but they can reasonably be expected to affect the coupling since the most significant anharmonicity occurs at the X point, just where the important phase space factor $\xi(q,\omega)$ peaks. This question requires further work beyond the scope of the present study.

E. Quasi-two-dimensionality

The possibility of achieving strong electron-phonon coupling without a large Fermi-level density of states is enhanced by the quasi-two-dimensionality (quasi-2D) of the cuprate superconductors. From Table IX it is clear that atomic displacements polarized perpendicular to the Cu-O layers tend to be very strongly coupled, no doubt partially the result of weak screening of the resulting electric fields. This effect is indirectly a result of the quasi-2D nature of the underlying band structure.

Another, more direct, implication of the quasi-2D electronic structure is the concentration of, or enhancement of, phase space for scattering by nesting,⁶⁴ by van Hove singularities,⁶⁵ or a combination thereof. These features have been noted above and are under more extensive study. However, a general feature of layered materials with quasi-2D Fermi surfaces is that scattering for all q along the axial direction will tend to have large phase space, since if $E(k)$ is on the Fermi surface, then $E(k+q)$ will also be on the Fermi surface. For a precisely 2D Fermi surface $\xi(q,\omega)$ will diverge for q along the axial direction; however in this limit the perpendicular bandwidth vanishes and the application of standard formulas must be reexamined. But before this limit is reached, scattering for axially directed q 's will be greatly enhanced. We suggest that neutron scattering should be applied to study this possibility.

F. Other calculations of electron-phonon coupling in high- T_c materials

Rodriguez *et al.*²¹ have also undertaken similar *ab initio* studies of the electron-phonon coupling strength in the high- T_c superconductors. Using the theory of Zehner and Zwicky⁶⁶ for small q phonon self-energies, they calculated the frequency shifts and broadenings of the five A_g optical phonons in $\text{YBa}_2\text{Cu}_3\text{O}_7$ upon cooling below T_c . Observed frequency shifts⁶⁷ and broadenings⁹ were found to be well accounted for by these calculations. Using a similar constant matrix element approximation, they obtained $\lambda \sim 1$, which is probably not big enough to account for T_c in $\text{YBa}_2\text{Cu}_3\text{O}_7$ but, of course, derives from only 5 of the 39 branches and only near $q \sim 0$. Andersen *et al.*²¹ also examined the fully symmetric S zone-corner phonons in $\text{YBa}_2\text{Cu}_3\text{O}_7$ and found relatively small

linewidths there. In Ref. 21 the matrix elements were obtained from splittings in the eigenvalues induced by the frozen-in phonon rather than by the direct calculation of the matrix elements of the change in the LDA potential that was used here. Electron-phonon matrix elements were also obtained by us⁴ from splittings of zone center phonons in $\text{YBa}_2\text{Cu}_3\text{O}_7$, and λ_v 's as large as 1.9 were found; the importance of long-range nonlocal contributions to the electron-phonon interaction were emphasized.

The importance of long-range interactions was also noted in a model calculation by Zehner¹⁵ for $\text{YBa}_2\text{Cu}_3\text{O}_7$. He used rigidly displaced ionic potentials that are screened by the dielectric background constant of the undoped material and by intraband scattering of holes confined to the CuO planes. The imperfectly screened long-range Coulomb interaction in this model gives rise to the large value⁵⁴ of $\lambda \sim 3$.

V. CONCLUSION

We have carried out frozen-phonon supercell calculations for $\text{La}_{2-x}\text{M}_x\text{CuO}_4$ using the LAPW method to determine the electron-phonon coupling strength for selected zone boundary and zone center phonons. We have used the local density functional and adiabatic approximation and have neglected anharmonic effects. Other than these, the calculations were fully *ab initio* and did not rely on further assumptions such as the rigid-ion

or rigid muffin-tin approximation. We have found moderate linewidths for O_{xy} breathing modes and O_z modes at the X point and a very large linewidth for the O_z mode at the Z point. It may be possible to observe this latter mode linewidth experimentally. If, however, there are nonmetallic phases present in the sample these phases would yield sharp phonon lines, and the broader signal from the superconducting phase may be overlooked as part of the background. An overall coupling strength was found that is sufficient to account for T_c without the need to augment this with coupling to other excitations. The calculated large electron-phonon coupling arises from a combination of weak screening and unusual nonlocal Madelung-like interactions, in concert with strong Cu-O hybridization that results in good metallic behavior within the planes. These features are common to all of the layered cuprates, indicating that the entire class should show strong electron-phonon coupling.

ACKNOWLEDGMENTS

We acknowledge useful discussions and communication with P. B. Allen, M. Cardona, K. McCarty, L. Pintchovius, and W. Reichardt. H.K. was supported by NSF Grant No. DMR-90-22588. W. E. P. acknowledges support from the Office of Naval Research. Computations were carried out at the Cornell National Supercomputing Facility and the Cray 2 at the National Center for Supercomputing Applications.

-
- ¹J. G. Bednorz and K. A. Müller, *Z. Phys. B* **64**, 189 (1986).
²W. E. Pickett, H. Krakauer, R. E. Cohen, and D. J. Singh, *Science* **255**, 46 (1992).
³*Theory of the Inhomogeneous Electron Gas*, edited by S. Lundqvist and N. H. March (Plenum, New York, 1983).
⁴R. E. Cohen, W. E. Pickett, and H. Krakauer, *Phys. Rev. Lett.* **64**, 2575 (1990); R. E. Cohen, W. E. Pickett, H. Krakauer, and D. A. Papaconstantopoulos, *Phase Transitions* **22**, 167 (1990).
⁵J. G. Bednorz and K. A. Müller, *Rev. Mod. Phys.* **60**, 585 (1988).
⁶C. Thomsen and M. Cardona, in *Physical Properties of High Temperature Superconductors I*, edited by D. M. Ginsberg, (World Scientific, Singapore, 1989), p. 409.
⁷M. V. Klein, *Physica C* **162-164**, 1701 (1989).
⁸T. Timusk, M. Reedyk, R. Hughes, D. A. Bonn, J. D. Garrett, J. E. Greedan, C. V. Stager, D. B. Tanner, F. Gao, S. L. Herr, K. Kamaras, G. A. Thomas, S. L. Cooper, J. Orenstein, L. F. Schneemeyer, and A. J. Millis, *Physica C* **162-164**, 841 (1989).
⁹B. Friedl, C. Thomsen, H.-U. Habermeier, and M. Cardona, *Solid State Commun.* **81**, 989 (1992).
¹⁰O. K. Andersen, *Phys. Rev. B* **12**, 3060 (1975); D. D. Koelling and G. O. Arbman, *J. Phys. F* **5**, 2041 (1975); D. R. Hamann, *Phys. Rev. Lett.* **42**, 662 (1979); E. Wimmer, H. Krakauer, M. Weinert, and A. J. Freeman, *Phys. Rev. B* **24**, 864 (1981); S.-H. Wei and H. Krakauer, *Phys. Rev. Lett.* **55**, 1200 (1985).
¹¹B. M. Klein and W. E. Pickett, in *Superconductivity in d- and f-Band Metals, 1982*, edited by W. Buckel and W. Weber (Kernforschungszentrum, Karlsruhe, 1982), p. 477.
¹²H. Krakauer, W. E. Pickett, and R. E. Cohen, *J. Supercond.* **1**, 111 (1988).
¹³T. Jarlborg, *Solid State Commun.* **67**, 297 (1988); **71**, 669 (1989).
¹⁴S. Barišić and J. Zelenko, *Solid State Commun.* **74**, 367 (1990); S. Barišić and I. Batistić, *Europhys. Lett.* **8**, 765 (1989).
¹⁵R. Zehner, *Z. Phys. B* **80**, 187 (1990).
¹⁶M. M. Dacorogna, M. L. Cohen, and P. K. Lam, *Phys. Rev. Lett.* **55**, 837 (1985); P. K. Lam, M. M. Dacorogna, and M. L. Cohen, *Phys. Rev. B* **34**, 5065 (1986).
¹⁷L. Pintchovius *et al.*, in *Proceedings of the International Seminar of High Temperature Superconductivity, 1989*, edited by V. L. Aksenov, N. M. Plakida, and V. Yu Yushankhai (Joint Inst. Nucl. Res., Dubna, 1990), p. 32; L. Pintchovius, in *Festkörperprobleme* (F. Vieweg and Son, Braunschweig, in press).
¹⁸W. Reichardt *et al.*, *Physica C* **162-164**, 464 (1989); W. Reichardt, *Neutron News* **1**, 20 (1990).
¹⁹R. E. Cohen, W. E. Pickett, and H. Krakauer, *Phys. Rev. Lett.* **62**, 831 (1989).
²⁰W. E. Pickett, R. E. Cohen, and H. Krakauer, *Phys. Rev. Lett.* **67**, 228 (1991).
²¹C. O. Rodriguez, A. I. Liechtenstein, I. I. Mazin, O. Jepsen, O. K. Andersen, and M. Methfessel, *Phys. Rev. B* **42**, 2692 (1990); O. K. Andersen, A. I. Liechtenstein, O. Rodriguez, I. I. Mazin, O. Jepsen, V. P. Antropov, O. Gunnarsson, and S. Gopalan, *Physica C* **185-189**, 147 (1991).
²²R. Manzke *et al.*, *Physica C* **162-164**, 1381 (1989); C. G. Olson *et al.*, *ibid.*, **162-164**, 1697 (1989); C. G. Olson *et al.*, *Phys. Rev. B* **42**, 381 (1990); J. G. Tobin *et al.*, *ibid.* **45**, 5563 (1992).

- ²³J. C. Campuzano *et al.*, Phys. Rev. Lett. **64**, 2308 (1990); Y. Sakisaka *et al.*, Phys. Rev. B **39**, 9080 (1989).
- ²⁴H. Krakauer and W. Pickett, Phys. Rev. Lett. **60**, 1665 (1988).
- ²⁵M. S. Hybertsen and L. F. Mattheiss, Phys. Rev. Lett. **60**, 1661 (1988).
- ²⁶S. Massidda, J. Yu, and A. J. Freeman, Physica C **52**, 251 (1988).
- ²⁷H. Krakauer, W. E. Pickett, and R. E. Cohen, J. Supercond. **1**, 111 (1988); W. E. Pickett, H. Krakauer, and R. E. Cohen, Phys. Rev. B **42**, 8764 (1990).
- ²⁸J. W. Allen and C. G. Olson, MRS Bull. **XV**, 34 (1990).
- ²⁹E. Dagotto, A. Moreo, F. Ortolani, J. Riera, and D. J. Scalapino, Phys. Rev. Lett. **67**, 1918 (1991).
- ³⁰H. Matsuyama, T. Takahashi, H. Katayama-Yoshida, T. Kashiwakura, Y. Okabe, and S. Sato, Physica C (Amsterdam) **160**, 567 (1989).
- ³¹T. Takahashi, H. Matsuyama, H. Katayama-Yoshida, K. Seki, K. Kamiya, and H. Inokuchi, Physica C (Amsterdam) **170**, 416 (1990).
- ³²J. W. Allen, C. G. Olson, M. B. Maple, J.-S. Kang, L. Z. Liu, J.-H. Park, R. O. Anderson, W. P. Ellis, J. T. Markert, Y. Dalichaouch, and R. Liu, Phys. Rev. Lett. **64**, 595 (1990).
- ³³R. Liu, B. W. Veal, A. P. Paulikas, J. W. Downey, H. Shi, C. G. Olson, G. Gu, A. J. Arko, J. J. Joyce, and R. J. Bartlett, Proceedings Workshop on Fermiology of High- T_c Superconductors, Argonne, March, 1991 [J. Phys. Chem. Solids **52**, 1437 (1991)].
- ³⁴T. Takahashi, S. Suzuki, T. Kusunoki, S. Sato, H. Katayama-Yoshida, A. Yamanaka, F. Mimani, and S. Takekawa, Physica C **185-189**, 1057 (1991).
- ³⁵P. B. Allen, Phys. Rev. B **6**, 2577 (1972).
- ³⁶S. Baroni, P. Giannozzi, and A. Testa, Phys. Rev. Lett. **58**, 1861 (1987).
- ³⁷H. Krakauer, R. E. Cohen, and W. E. Pickett, Mat. Res. Soc. Symp. Proc. **141**, 165 (1989).
- ³⁸W. H. Butler, F. J. Pinski, and P. B. Allen, Phys. Rev. B **19**, 3708 (1979).
- ³⁹N. Wakabayashi, Phys. Rev. B **33**, 6771 (1986).
- ⁴⁰T. C. Leung, X. W. Wang, and B. N. Harmon, Phys. Rev. B **37**, 384 (1988).
- ⁴¹J.-H. Xu, T. J. Watson-Yang, J. Yu, and A. J. Freeman, Phys. Lett. A **120**, 489 (1987).
- ⁴²W. E. Pickett, H. Krakauer, and R. E. Cohen, Physica B **165-166**, 1055 (1990).
- ⁴³P. B. Allen, Phys. Status Solidi B **120**, 529 (1983).
- ⁴⁴W. E. Pickett, H. Krakauer, and P. B. Allen, Phys. Rev. B **38**, 2721 (1988).
- ⁴⁵J. M. Longo and P. M. Raccach, J. Solid State Chem. **6**, 526 (1973).
- ⁴⁶L. Pintschovius *et al.*, Physica C **185-189**, 156 (1991).
- ⁴⁷W. H. Weber *et al.*, Phys. Rev. B **38**, 917 (1988); Solid State Commun. **68**, 61 (1988).
- ⁴⁸I. Ohana *et al.*, Phys. Rev. B **39**, 2293 (1989).
- ⁴⁹P. Boni *et al.*, Phys. Rev. B **38**, 185 (1988).
- ⁵⁰C. Falter, M. Klenner, and W. Ludwig, Phys. Lett. A **165**, 260 (1992).
- ⁵¹P. B. Allen and R. C. Dynes, Phys. Rev. B **12**, 905 (1975).
- ⁵²M. Gurvitch and A. T. Fiory, Phys. Rev. Lett. **59**, 1337 (1987).
- ⁵³I. I. Mazin and O. V. Dolgov, Phys. Rev. B **45**, 2509 (1992).
- ⁵⁴R. Zeyher, Phys. Rev. B **44**, 10404 (1991).
- ⁵⁵V. H. Crespi and M. L. Cohen, Solid State Commun. **81**, 187 (1992).
- ⁵⁶C. T. Chen, L. H. Tjeng, J. Kwo, H. L. Kao, P. Rudolf, F. Sette, and R. M. Fleming, Phys. Rev. Lett. **68**, 2543 (1992).
- ⁵⁷W. E. Pickett, H. Krakauer, D. A. Papaconstantopoulos, and L. L. Boyer, Phys. Rev. B **35**, 7252 (1987).
- ⁵⁸G. Bergman and D. Rainer, Z. Phys. **263**, 59 (1973); P. B. Allen, Solid State Commun. **14**, 937 (1974).
- ⁵⁹J. D. Axe *et al.*, Phys. Rev. Lett. **62**, 2751 (1982).
- ⁶⁰A. R. Moodenbaugh *et al.*, Phys. Rev. B **38**, 4596 (1988); T. Suzuki and T. Fujita, J. Phys. Soc. Jpn. **58**, 1883 (1989).
- ⁶¹W. Reichardt *et al.*, Physica C **162-164**, 1701 (1989).
- ⁶²J. D. Axe *et al.*, in *Proceedings of Lattice Effects in High- T_c Superconductors*, edited by Y. Bar-Yam, T. Egami, J. Mustre-de Leon, and A. R. Bishop (World Scientific, Singapore, 1992).
- ⁶³R. E. Cohen, W. E. Pickett, D. Papaconstantopoulos, and H. Krakauer, in *Proceedings of Lattice Effects in High- T_c Superconductors* (Ref. 62).
- ⁶⁴J. Ruvalds and A. Virosztek, Phys. Rev. B **43**, 5498 (1991).
- ⁶⁵R. S. Markiewicz, Physica C **169**, 63 (1990), and references therein; C. C. Tsuei, D. M. Newns, C. C. Chi, and P. C. Pattnaik, Phys. Rev. Lett. **65**, 2724 (1990).
- ⁶⁶R. Zeyher and G. Zwircknagl, Z. Phys. B **78**, 175 (1990).
- ⁶⁷C. Thomsen, M. Cardona, B. Friedl, C. O. Rodriguez, I. I. Mazin, and O. K. Andersen, Solid State Commun. **75**, 219 (1990).

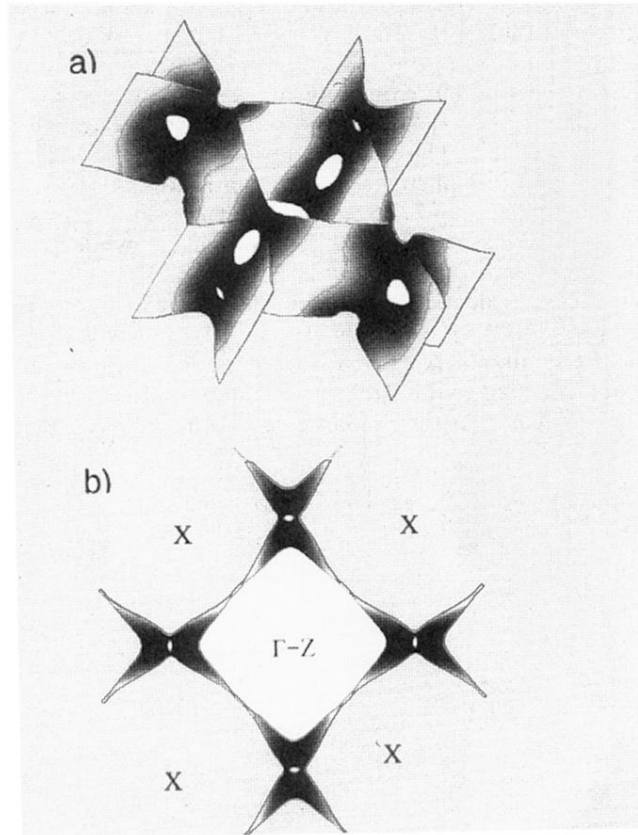


FIG. 1. Two views of the Fermi surface for $\text{La}_{1.85}\text{M}_{0.15}\text{CuO}_4$. (a) The shaded areas indicate low-velocity regions near the van Hove singularities at the corners. (b) The Γ -Z axis is perpendicular to the page in this view, which indicates the degree of smearing of the van Hove singularities due to k_z dispersion.